

NeRF-To-Real Tester: Neural Radiance Fields as Test Image Generators for Vision of Autonomous Systems

Laura Wehl
IT University of Copenhagen
Copenhagen, Denmark
lawe@itu.dk

Bilal Wehbe
Robotics Innovation Centre, DFKI
Bremen, Germany
bilal.wehbe@dfki.de

Andrzej Wąsowski
IT University of Copenhagen
Copenhagen, Denmark
wasowski@itu.dk

Abstract—Autonomous inspection of infrastructure on land and in water is a quickly growing market, with applications including surveying constructions, monitoring plants, and tracking environmental changes in on- and off-shore wind energy farms. For Autonomous Underwater Vehicles and Unmanned Aerial Vehicles overfitting of controllers to simulation conditions fundamentally leads to poor performance in the operation environment. There is a pressing need for more diverse and realistic test data that accurately represents the challenges faced by these systems. We address the challenge of generating perception test data for autonomous systems by leveraging Neural Radiance Fields to generate realistic and diverse test images, and integrating them into a metamorphic testing framework for vision components such as vSLAM and object detection. Our tool, N2R-Tester, allows training models of custom scenes and rendering test images from perturbed positions. An experimental evaluation of N2R-Tester on eight different vision components in AUVs and UAVs demonstrates the efficacy and versatility of the approach.

Index Terms—neural radiance fields, autonomous systems, metamorphic testing

I. INTRODUCTION

“*I am not crazy; my reality is just different from yours.*” says the Cheshire Cat [1]. A roboticist might conclude that the Cheshire cat experiences the *simulation-to-reality gap*; the gap between the confines of system’s own objective reality, and the complexities of the real world. For Autonomous Underwater Vehicles (AUVs) and Unmanned Aerial Vehicles (UAVs) overfitting on simulation-based testing setups fundamentally leads to poor performance in the operating conditions of the real world. Testing research aims to decrease the gap.

Autonomous inspection of infrastructure both underwater and on land is a quickly growing market, with example applications including surveying buildings and bridges, processing plants, and tracking environmental changes in on- and off-shore construction sites or wind energy farms. Robotic inspections facilitate automatic detection of material degradation, initialisation of preventative measures to avoid equipment damage, as well as scheduling timely maintenance operations. To enable safe autonomous operations in real-world environments with potentially adverse weather conditions such as wind or underwater currents, we need to establish the quality of different algorithmic implementations used for navigation, and ensure their reliability of establishing a consistent understanding of their environment.

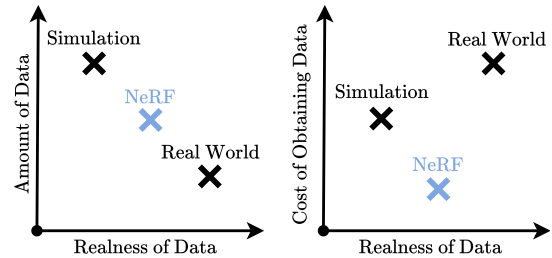


Fig. 1: Trade-offs between the realness and amount of data.

AUV missions can extend over long time and distance, which increases the risk of drift and pose estimation errors due to underwater currents and sensor failures [2]. Integrating image-based perception into the navigation stack can reduce these failures and enhance the AUV’s real-time understanding of the scene. Consider an example subsystem in a typical vision stack: An Interest Point Detector (IPD) is used during visual simultaneous localisation and mapping (vSLAM) to track the AUV’s position in an open environment. Like many vision components, IPDs are negatively affected by the adverse conditions underwater such as bad visibility or sudden positional changes due to underwater currents. Similarly, in aerial surveillance, accurate object detection and classification are crucial for safe mission completion. Light-weight Deep Neural Networks (DNNs) can be deployed on modern UAVs, such as quadcopters, to run real-time image classification, facilitating adaptive decision making for object tracking and obstacle avoidance. Sudden adverse wind turbulence can cause an UAV to fall short in their understanding of the scene. Unfortunately, despite the importance of IPDs and classifiers for safety of the autonomous vehicles, existing methods for testing such components fall short in generating real and diverse image data that exposes the system under test to realistic dynamics.

For generating test data, simulators offer controlled environments and the ability to manipulate lighting conditions and scene characteristics. However, their effectiveness is constrained by the expertise and domain knowledge of the engineers who design them. A good performance on a simulation benchmark does not necessarily guarantee a good performance in the real world, hence the expression “simulation-to-reality gap”. Additionally, simulators often fail to encompass the full spectrum of

unexpected safety-critical scenarios that may arise in real-world environments. Consequently, there is a pressing need for more diverse and realistic test data that accurately represents the challenges faced both by AUVs and UAVs. A trend in 3D scene reconstruction has emerged in recent years known as Neural Radiance Fields (NeRFs) [3], which establish a differentiable environmental representation by training a fully connected network on camera images and their poses. This allows to render new views from the learned scene, by querying a camera pose. This positions NeRFs as a source of more realistic test data when compared to manually engineered simulations, placing them at a sweet spot between simulated and real data when it comes to amount and cost of obtaining data (Fig. 1).

We address the challenge of diversity and realness of perception test data for autonomous vehicles by leveraging NeRFs to generate realistic and diverse test images, with a specific focus on vision components such as vSLAM in AUVs and obstacle detection in UAVs. We adopt a metamorphic testing (MT) framework to uncover inconsistencies in several systems under test (SUT) using the NeRF-generated data. Specifically, we contribute:

- A short analysis of requirements and the existing methods for generating visual test data for autonomous systems (Sect. III),
- An adaptation of metamorphic testing to testing vision components in 3D space on real and NeRF-generated data (Sect. IV),
- NeRF-to-Real-Tester (N2R-Tester), an implementation including NeRF training and image rendering¹,
- An experimental evaluation of N2R-Tester on eight different vision components in AUVs and UAVs, demonstrating the efficacy and versatility of the approach (sections V and VI).

II. BACKGROUND

Neural Radial Fields [3] are function approximations of the form $\theta : (\mathbb{R}^3, \mathbb{R}^2) \rightarrow (\mathbb{R}^3, \mathbb{R})$. Given a set of images with associated 3D locations \mathbf{x} and viewing angles \mathbf{d} of one particular scene or object, a NeRF learns to map $\theta(\mathbf{x}, \mathbf{d}) \rightarrow (\mathbf{c}, \sigma)$, where the output \mathbf{c} is the emitted RGB colour and σ is the volume density. See Fig. 2 for an overview of the NeRF training and rendering process. A trained NeRF model is able to render new views of a scene from previously unseen viewpoints, i.e. combinations of (\mathbf{x}, \mathbf{d}) . This is achieved by standard volumetric rendering techniques, i.e. a ray \mathbf{r} is “fired” from the camera origin \mathbf{o} , as shown in Fig. 2. When tracing the ray between the near and far bounds t_n, t_f and taking samples along the ray at different points t , the expected colour $C(\mathbf{r})$ of this ray $\mathbf{r}(t) = \mathbf{o} + t\mathbf{d}$ starting at the camera origin \mathbf{o} is given by:

$$C(\mathbf{r}) = \int_{t_n}^{t_f} \text{Tr}(t)\sigma(\mathbf{r}(t))\mathbf{c}(\mathbf{r}(t), \mathbf{d}) dt. \quad (1)$$

The function $\text{Tr}(t)$ represents the probability of the ray travelling through σ without being obstructed by any particle:

$$\text{Tr}(t) = \exp\left(-\int_{t_n}^t \sigma(\mathbf{r}(s))ds\right) \quad (2)$$

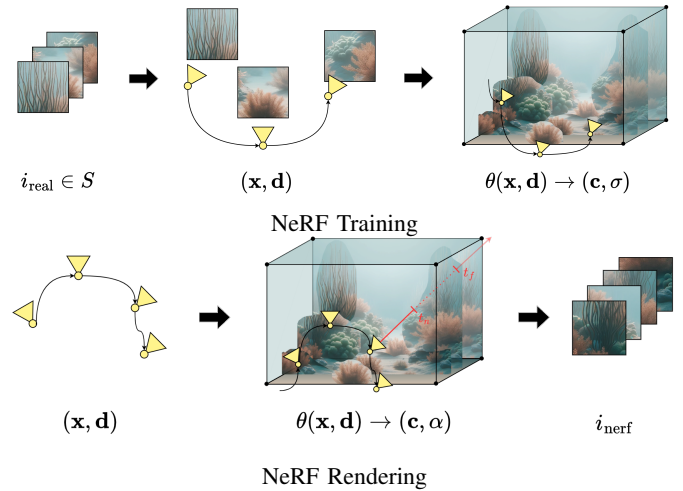


Fig. 2: (Top) We take a set of real images of a scene $i_{\text{real}} \in S$ as input. The NeRF model θ learns to map the estimated camera poses \mathbf{x}, \mathbf{d} (yellow) to colour \mathbf{c} and volumetric density σ . (Bottom) We pass new camera poses (\mathbf{x}, \mathbf{d}) to the NeRF model θ , creating previously unseen views i_{nerf} of the scene. Camera rays $\mathbf{r}(t)$ (red) are projected from the camera origin along the trajectory between a near and far bounds t_n and t_f .

Note that NeRF models are unusual comparing to most other deep learning models; instead of learning patterns in a data set to enable generalisations or classifications the aim here is to learn a 3D scene representation by overfitting to a particular single scene or object.

III. WHAT IS A GOOD TEST IMAGE?

Producing valid test images for perception subsystems is an active and challenging research area. It involves generating input images that preserve photometric, semantic, geometric and other contextual information while introducing perceivable, realistic as well as diverse changes, for which we are still able to determine the expected test output. Especially for navigation applications such as vSLAM, spatio-temporal consistency is vital to preserve geometric information across consecutive frames under pose translations. Therefore, we outline three key requirements for the generation of test images, that allow us to confidently assess the reliability of a system in real-world scenarios:

Realness: Generated test images are comparable to real scene images from the operational domain,

Diversity: Generated test images add value to the available training data, so they differ from the training data,

Spatio-Temporal Consistency: Consecutive images representing agent’s motion present consistent geometry.

These are interconnected requirements on test image data that ensure a robust and comprehensive testing of perception systems for navigation. Without realness we cannot confidently assess the reliability of a system in real-world scenarios. Without diversity we cannot test generalisation. Without spatio-temporal consistency, testing of a navigational systems is void.

¹DOI: 10.5281/zenodo.14251863

a) *Realness*: Strictly speaking, valid test inputs for testing perception are the images of real world scenes as captured by a representative camera. Methods like cross-validation enable model evaluation with images from operational conditions. However, using only real world scene data is often too costly. For instance, in underwater robotics, acquiring data necessitates offshore missions, involving considerable resources and time. Therefore, alternative methods are necessary to obtain additional yet realistic images. One possibility is to resort to simulation [4]. Unfortunately, the images produced by simulators are still not sufficiently realistic. They are presently more useful for pre-training perception models, and for visual assessment of robot actions by humans. Adversarial methods create imperceptibly small noise vectors that, when added to a real image, push it over a decision boundary [5]. Similarly, coverage-based methods that generate images triggering faulty behaviour, are inherently adversarial, focusing on the model rather than the operational domain distribution [6], [7], [8]. The adversarial inputs are realistic from the human eye perspective and may pose a significant threat from a security point of view. However, they are not realistically producible by representative cameras in operational scenes, so they are not interesting for testing robustness of perception. For these reasons, we study NeRFs, a model designed for realistic representation of scenes.

b) *Diversity*: Test data generation aims to extend beyond the training data, while maintaining realness. Simple methods like rotating and scaling images, known as data augmentation, are common in DNN training. Most of the existing research on the diversity of the generated data focuses on more advanced transformation techniques and on measuring realness or validity of the generated inputs. One group of methods patches existing images; pasting new objects and changing properties of objects (e.g. lighting or colour [9]). However, these can be easily identified as unreal by humans. A less direct approach is to perform search in the feature space [10], [11], or to train Generative Adversarial Networks (GANs) which produce images that appear realistic. GANs have also been used to change global properties of an image, like weather conditions [12]. A GAN incorporates a discriminator network which optimises the realness of the generated images. Crucially, the discriminator network learns statistical patterns and not the semantic content in the generated images. It might learn to exploit weaknesses in the discriminator without actually learning how to represent the underlying distribution and therefore alternative methods are still needed. Other methods such as training Variational Autoencoders (VAEs) [13] and using their reconstruction probabilities as proof for validity is not effective because each model’s output is conditioned on its own dataset’s characteristics. Comparing these probabilities are not directly comparable since they are relative to their underlying distributions. Proxy metrics are typically used to evaluate realness of images produced by generative models. Peak-Signal-To-Noise Ratio (PSNR) is based on the mean squared error, and therefore sensitive to rotations, which otherwise have little impact on human perception of realness. Structural Similarity Index (SSIM) estimates structural similarity between two images according

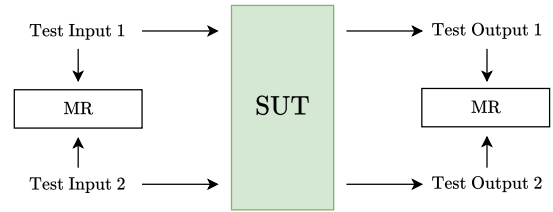


Fig. 3: Metamorphic testing: We establish metamorphic relations (MR) between pairs of test inputs and between the corresponding outputs. The test fails if the latter do not hold.

to luminance and contrast [14]. Learned Perceptual Image Patch Similarity (LPIPS) measures similarity in a DNN feature representation [15]. Unlike the above, we use transformations in the NeRF space (rolls and translations) to create new inputs for the perception components. Instead of challenging the SUT with new object and lighting configurations, we generate new view angles and new occlusions.

c) *Spatio-temporal Consistency*: For testing perception in the context of navigation, one needs to produce pairs, or sequences, of images that differ in the camera location, and that manifest the corresponding changes to the geometry of objects in the scene—consistent variation of positions, view angles, and occlusions. NeRFs were originally developed precisely for this requirement. Unlike GANs, where the learned distribution is a complex manifold in a high-dimensional space, giving poor control in the image generation process, NeRFs can render new images parameterised with camera positions in Euclidian space. This allows to emulate the motion of the agent, while maintaining the realness driven by the training data in the scene.

IV. METHOD

We describe our method to use NeRFs as test image generators within a customised metamorphic testing procedure.

A. Metamorphic Testing

Metamorphic Testing (MT) is a testing framework to assess the accuracy and robustness of a System Under Test (SUT) [16]. It is particularly well-suited when the quality of the expected output of a SUT is difficult to establish due to high dimensionality of the test data or absence of ground truth. Unlike traditional testing methods that rely on input-output pairs, in MT we formulate metamorphic relations (MRs) between input-input and output-output pairs that the SUT is expected to comply with (Fig. 3). MT therefore aims to capture the intrinsic properties of the data that the system processes. While other testing techniques aim at detecting bugs on a code level, MT can uncover critical inconsistencies on a behavioural level of a SUT by observing discrepancies in test outputs, given interrelated test inputs. MT is highly suitable for testing image-based perception systems where the inherent complexity and unstructured nature of image data poses significant challenges. Given a SUT f that processes images i of a scene S , a metamorphic relation can be expressed as:

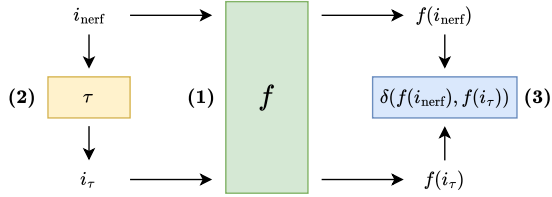


Fig. 4: N2R-Tester: (1) an image processing SUT f , (2) a metamorphic relation (MR) in form of a pose transformation τ rendered in a NeRF model, (3) an MR δ checking inconsistencies between the outputs $f(i_{\text{nerf}})$, $f(i_{\tau})$ of the SUT.

$$\forall i \in S. f(g_I(i)) = g_O(f(i)) . \quad (3)$$

Here, g_I, g_O are functions that transform the programme input and output domain of f respectively. We transform the test images i according to function g_I to generate new tests and validate them against the output of the SUT $f(i)$ by function g_O . In this work, we utilise NeRFs as automatic test image generators g_I while simultaneously monitoring the effects that NeRF-generated images have on the output of a SUT (Fig. 4). To achieve this we employ a range of transformations of an input image as our input MR and evaluate discrepancies between the outputs of the SUT for the transformed images using performance metrics (Fig. 5). The strength of NeRFs lies in their ability to render realistic images from previously unseen camera poses (\mathbf{x}, \mathbf{d}) of a scene or object, while preserving its photometric, structural and geometric information, which simultaneously offers image diversity by giving different viewpoints. We exploit this ability by applying a range of transformations T to (\mathbf{x}, \mathbf{d}) in the 3D NeRF space. We denote the a transformed image i_{τ} . We report how a SUT f responds to a range of diverse test images by the amount of $\delta(f(i_{\text{nerf}}), f(i_{\tau}))$. The predicate INC below captures the violation written using a performance metric q into real numbers:

$$\text{INC}(f) = q(f(i_{\text{nerf}}), f(i_{\tau})) > \epsilon \quad (4)$$

B. NeRF-To-Real Tester

N2R-Tester $\langle f, S, T, \delta \rangle$ comprises a system under test f , a set of images S of a scene or object, a list of pose transformations T , and metamorphic relations δ . N2R-Tester takes the image set S and reconstructs a 3D scene solely based on these 2D input images in form of a NeRF model. We achieve this by feeding all images $i \in S$ to a structure-from-motion (SfM) component, colmap [17], which selects a subset of all images $S_{\text{real}} \subseteq S$ to get estimated camera poses (\mathbf{x}, \mathbf{d}) for each image in $i_{\text{real}} \in S_{\text{real}}$. These image/camera-pose combinations are used to train a NeRF model θ . Now we render the same camera poses in the NeRF model to get all corresponding NeRF-generated images i_{nerf} from the identical viewpoints. Subsequently, we apply a number of different transformations $\tau \in T$ to each of the camera poses (\mathbf{x}, \mathbf{d}) to render the transformed images in the NeRF model to get i_{τ} . The supported transformations are translations of position as well as rotations in roll, pitch and yaw angle.

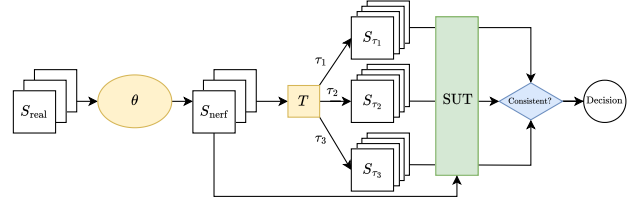


Fig. 5: N2R-Tester Process: Given a set of real images of a scene S_{real} we train a NeRF model θ . By designing a set transformations T we can generate a high number of additional test images and check the consistency of the SUT behaviour.

V. EXPERIMENTAL EVALUATION

We evaluate N2R-Tester experimentally, in two application scenarios: (1) testing an interest point detector of an AUV during a wall inspection mission, and (2) testing an image classifier in an UAV during a vehicle inspection mission. Both scenarios require operating in a 3D space with 6 degrees of freedom, i.e. in air and in water, as well as their exposition to air or water turbulence causing abrupt positional jumps which challenge the understanding of the scene. Specifically, we pose the following research questions (RQs).

- **RQ1:** How effective is N2R-Tester at generating *realistic* images of a scene or object as perceived by an image processing SUT?
- **RQ2:** How effective is N2R-Tester at generating *diverse* images of a scene or object that uncover inconsistent behaviours in an image processing SUT?
- **RQ3:** How efficient is N2R-Tester at detecting inconsistencies in the behaviour of an image processing SUT?

Research questions RQ1 and RQ2 address the two core requirements of Sect. III. The spatiotemporal consistency is satisfied by-design, and it is evaluated in NeRF papers.

A. Training Data

a) *AUV Wall Inspection:* We record five videos of underwater scenes using a manually operated underwater drone equipped with a single front-facing camera. We mimic a trajectory of an AUV during inspections of vertical planar walls. Each video lasts approximately one minute. Images are extracted at 25 FPS and the resolution of 1920×1080 . The scenes contain walls covered by various types of marine growth. We estimate the camera poses with colmap [17] (see Tbl. I).

b) *UAV Vehicle Inspection:* We use two image data sets available in nerfstudio [18] (plane, dozer), that are captured with a handheld camera device. The nerfstudio data sets contain images and estimated camera poses for each image. We record three additional scenes with a handheld camera, containing a car, a truck and a bike and extract images at 25 FPS with image resolution of 1920×1080 pixels. We again use colmap for camera pose estimation. The images of all data sets have the respective vehicle roughly at the image centre and the camera trajectory mimics a UAV circling around the vehicle at an approximately fixed level above ground. See also Tbl. I.

NeRF Model	Mission	Image Resolution	#Total Images	#Train Images	Train Time(h)
dory1	AUV	1920×1080	301	271	1.38
dory2	AUV	1920×1080	330	297	1.88
dory3	AUV	1920×1080	358	323	1.39
dory4	AUV	1920×1080	303	273	1.52
dory5	AUV	1920×1080	356	321	1.41
plane	UAV	1080×1920	317	286	1.68
dozer	UAV	3008×2000	359	324	1.38
car	UAV	1920×1080	532	479	1.28
truck	UAV	1920×1080	418	377	1.39
bike	UAV	1920×1080	303	273	1.31

TABLE I: Training data sets. Each of the #total images has an associated camera pose estimation. 90% are used for NeRF training. 10% are used for NeRF in-training evaluation.

B. Systems Under Test

a) *Interest Point Detectors (AUV)*: We evaluate N2R-Tester on four AUV components as SUTs: two DNN-based IPDs as well as two popular state-of-the-art non-DNN IPDs.

- **SuperPoint**: SuperPoint, a convolutional DNN, predicts interest points by calculating heatmaps of likely interest point locations. It is trained on a large dataset with partially manual and automatically labelled ground truth data [19].
- **UnSuperPoint**: UnSuperPoint is a DNN-based IPD, that incorporates point regression and a mechanism similar to Non-maximum suppression directly in its architecture which helps finding evenly distributed interest points across an image. It is trained in a self-supervised fashion [20].
- **Scale-Invariant Feature Transform (SIFT)**: SIFT finds interest points in an image by convolving Gaussian kernels at different scales across the image and subsequently selecting local extrema in difference-of-Gaussian pyramids [21].
- **Oriented FAST and Rotated BRIEF (ORB)**: ORB is based on the FAST point detector, which measures local gradients in pixel intensities in circular patches around each pixel [22].

We use the OpenCV implementations of SIFT and ORB [23]. SuperPoint with pre-trained weights is available on github [24]. UnSuperPoint is proprietary software and currently not publicly available with pre-trained weights. We obtained it from the authors.

b) *Image Classifiers (UAV)*: We evaluate N2R-Tester on four UAV components as SUTs; two small DNNs with ~4-5M parameters, selected for their capacity to be deployed on modern quadcopters, as well as two large DNNs. We choose MobileNet [25], EfficientNet [26], Xception [27] and VGG16 [28], all as implemented in Keras [29]. All models have a convolutional architecture and are trained on ImageNet-1k [30]. Each image is downsampled to a model-specific resolution. We use a recommended downsampling method of OpenCV, namely “inter-area” downsampling. See Tbl. II.

C. Performance Metrics for Systems Under Test

We consider a total of four SUT metrics, three for the UAV mission and two for the AUV mission, and inject them into our MT framework:

- **Image Classification: Cosine Similarity \uparrow** : The final layer of a DNN produces predictions for each class in the data set.

DNN Model	Size	Input Res.	Top-1 Acc.	#Params
MobileNet	16	224×224	70.4%	4.3M
EfficientNetB0	29	224×224	77.1%	5.3M
Xception	88	299×299	79.0%	22.9M
VGG16	528	224×224	71.3%	138.4M

TABLE II: Subject classifier SUTs, data after Keras [31]. Size is for a file of pre-trained weights in MB. Each DNN uses a specific input layer resolution. The top-1 accuracy refers to the accuracy on the ImageNet-1k validation set.

As our UAV SUTs are trained on a subset of ImageNet with 1k classes, the output of the DNN is a vector of 1000 scores. The cosine similarity is a measure of similarity between two DNN outputs. It is the cosine angle between the two vectors; two parallel vectors have a cosine similarity of 1, two orthogonal vectors have a cosine similarity of -1.

- **Image Classification: L2 Norm \downarrow** : The final layer of the DNN produces predictions for each class in the data set. As our UAV SUTs are trained on a popular subset of ImageNet with 1k classes, the output of each DNN is a vector of 1000 scores. The L2 norm between two DNN outputs is the Euclidean squared distance between the two output vectors.
- **Image Classification: Class Invariance \uparrow** : When comparing two different images and their respective DNN output vectors, we consider whether the highest probability is given to the same class. We define class invariance as the percentage of images in a set where two prediction vectors have the highest probability for the same class.
- **IPD: Repeatability Score \uparrow** : To report the performance IPDs we use the repeatability score between two sets of interest points. By calculating a homography between two images of the same scene, we can project the first set of interest points onto a second image and find the percentage of matched points [32]. We allow a maximum distance of 2 pixels to consider two points a match.
- **IPD: Interest Point Spread \uparrow** : As an intuitive measure of the quality of interest points, we calculate their Jaccard Index, i.e. the ratio between the intersection and union of the areas that the interest points cover in an image. A distribution across an image is a desired property of interest points to improve stability [33].

D. NeRF Models

The structure-from-motion tool colmap selects a minimum 300 suitable images of a captured scene by balancing sufficient visual information and processing speed. Colmap subsequently estimates the camera poses for each image. For our NeRF models we choose a network architecture called Nerfacto, available in nerfstudio [18] because of its balance between training/rendering speed and visual quality. The NeRF training process takes 90% of image/camera-pose combinations to learn each scene by updating its network weights. The remaining 10% are left out for NeRF in-training-evaluation on image fidelity metrics PSNR, SSIM, LPIPS continuously during the training process. We train a total of ten NeRF models on underwater and aerial scenes listed in Tbl. I. We predominantly used the default parameters in nerfstudio to

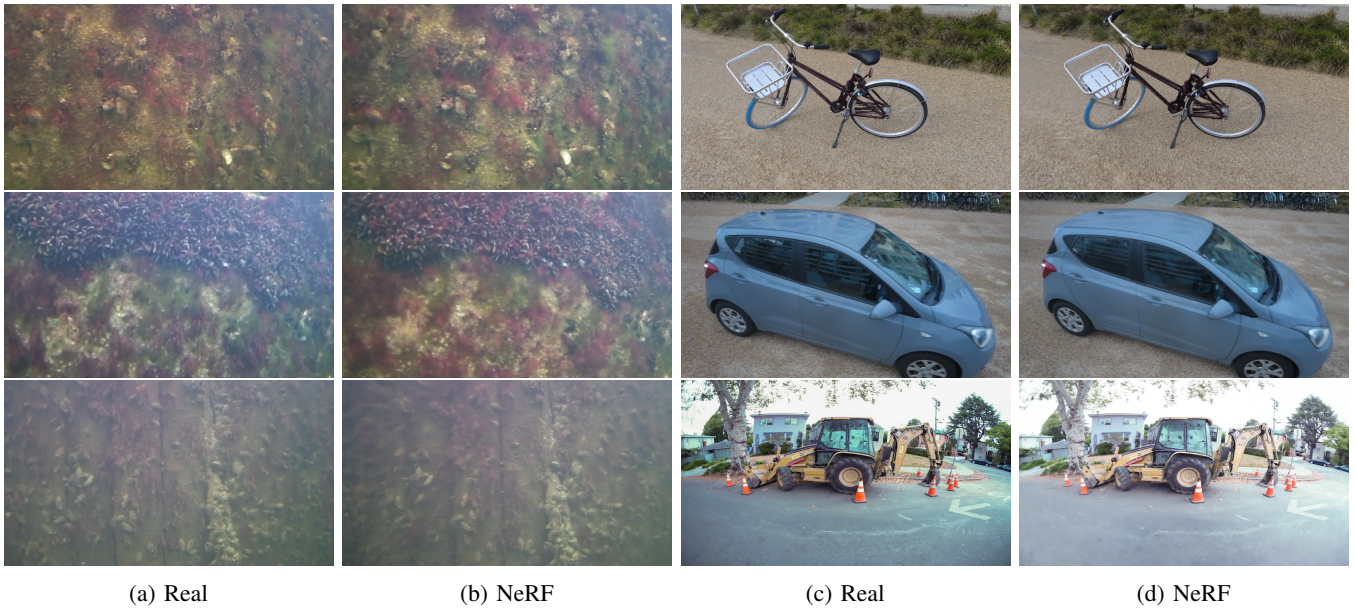


Fig. 6: Visual quality of NeRF-generated images: (a) Real images of three underwater scenes of an AUV wall inspection mission. (b) NeRF-generated pose-equivalent images as (a) in the respective NeRF models `dory1`, `dory2` and `dory3`. (c) Real images of three scenes of an UAV vehicle inspection mission. (d) NeRF-generated pose-equivalent images as (c) in the respective models `bike`, `car` and `dozer`.

train our models with a fixed number of 30k training steps where each training step comprises 4096 ray samples.

E. Evaluation for N2R-Tester

In order to demonstrate the efficacy of N2R-Tester in producing realistic and diverse test images, and thus answering RQ1, RQ2, and RQ3, we inject our SUTs, NeRF models and MRs into our framework. Additionally, we employ artificial image mutations suggested by authors of DeepXplore [6] to enable a baseline comparison. Note that in their work, the image mutations are used to generate test images to find DNN test inputs that trigger differential SUT behaviour and cause high neuron coverage. We are not interested the neuron coverage metric since it has shown inconclusive efficacy in other works [34]. We still choose the DeepXplore mutations because they are engineered artificially, thus we are curious to their level of realism and comparative output in SUT behaviour.

VI. RESULTS

In this section, we discuss the experiment results of N2R-Tester, and its ability to test our SUTs, i.e. interest point detectors and image classifiers. All test images are rendered at a resolution of (960, 540, 3) pixels.

A. RQ1: Realness

a) Visual quality of NeRF-generated images: Figure 6 shows a range of real and NeRF-generated images of underwater and vehicle scenes to convince the reader of the visual quality of images produced by rendering an image with a NeRF. The images generated by the underwater models `dory1`, `dory2` and `dory3` demonstrate an almost indistinguishable resemblance with the real world scene, with a relatively

small loss in visual definition of specific features. The images produced by `bicycle`, `car` and `dozer` show a similar visual quality and convince by rendering subtle details with consistency, for example in the bicycle spokes in `bicycle`. Some short-comings can be seen in the foreground of `dozer` in the slightly under-defined representation of the street tarmac.

The NeRF reconstruction process is initialised with random pixels, which gradually converge to a geometrically consistent scene during training. During inference this presents an advantage; NeRFs fail gracefully when faced with ambiguity in the reconstruction, i.e. when rendering an image at a view with insufficient radiance samples. This can however result in “artifacts” or “ghost walls”, i.e. image patches appearing as random noise or blurry (Fig. 12). We find that an effective test for detecting ghost walls in a NeRF image is if an IPD returns fewer than the preset number of interest points, in our case 100. Researchers in the NeRF community are in a race trying to outperform each other in mitigating these pixel effects [35]. Nerfacto models assume the real-world scenes to be static, but other types of NeRF architectures aim at modelling dynamic scenes [36], [37]. Additionally, NeRFs assume that the real-world scene contains one main light source, and they tend to struggle in reconstructing surfaces and objects that reflect light such as mirrors and glass surfaces. Figure 12 exemplifies a few of these phenomena. We are curious as to how exactly these phenomena potentially affect the performance of the SUTs, however this exploration marks a whole line of research in its own right. We found the near and far bound parameters t_n , t_f in Eq. (1) supported convergence during the reconstruction process for `dory1` and `dory3` based on evaluation loss. We report the image metrics PSNR, SSIM and LPIPS for each scene

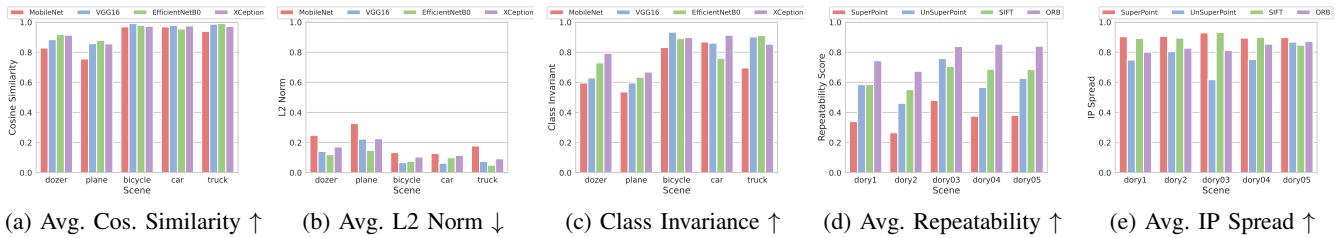


Fig. 7: Performance comparison of SUTs under the reality-to-NeRF domain shift in pose-equivalent images in S_{real} and S_{nerf} .

in Fig. 8 in blue. Notice that worse scores on the image metrics for `dozer` and `plane` correlate with worse scores on the SUT metrics in Fig. 7. Transformations τ often present on average equal or higher values for PSNR and LPIPS than DeepXplore mutations, and hence suggest a higher level of realism.

b) SUT Performance under reality-to-NeRF domain shift:

We investigate the sensitivity of each SUT to the domain shift from real to NeRF-generated images according to the selected SUT metrics. We consider the set of real images S_{real} and their pose-equivalent counterparts in S_{nerf} (e.g. Fig. 6 first column compared to second column). The significance of the SUT metric values under the domain shift is twofold; it can be seen as 1) a measure of quality in the NeRF reconstruction and realism of NeRF-generated images, and 2) an indication of relative performance of each SUT when presented with visually similar content but small pixel perturbations. See Fig. 7 for average values of each SUT metric in their respective UAV/AUV application. If we passed the exact same image to any SUT, we would expect a value of 1 for cosine similarity, class invariance, repeatability and IP spread, as well as a value of 0 for the L2 Norm. Any deviation of these values can be seen as an indication of the two properties described above. For each UAV scene, MobileNet shows the lowest scores throughout 13/15 settings compared to other SUTs. ORB is the IPD with the most consistent interest points under the domain shift in all AUV scenes according to the repeatability metric. The interest points of SuperPoint and SIFT appear to find interest points in the most consistent areas compared to the other SUTs. The models `dozer` and `plane` consistently show an overall lower levels of realism in the reconstruction, considering all SUTs show lower scores for these models in all settings.

c) Statistical Dependence between Image Quality Metrics and SUT Metrics:

We are curious whether the image quality metrics PSNR, SSIM, LPIPS have correlation with the UAV/AUV-associated SUT metrics under the reality-to-NeRF domain shift. We consider the real images S_{real} and their pose-equivalent images in S_{nerf} . Intuitively, the better an image i_{nerf} is reconstructed, i.e. has better values for PSNR, SSIM and LPIPS, then the features between pairs of i_{real} and i_{nerf} should also have higher agreement, and therefore higher SUT metrics. Thus the images show a higher level of realism. We find there is significant dependence for 38 out of 48 SUT metric / image quality metric combinations as seen in Tbl. III, based on Spearman rank correlations up until a p-value of 0.05.

B. RQ2: Diversity

Since each NeRF model has its own scale, we design targeted pose transformations for each NeRF model individually. We consider the reality-to-NeRF domain shift a transformation in itself and call it τ_0 . We additionally perform six types of pose transformations in the NeRF model:

- τ_0 : reality-to-NeRF domain shift,
- τ_1 : small translation on x-axis, small rotation in yaw,
- τ_2 : small translation on y-axis, small rotation in pitch,
- τ_3 : large translation on x-axis, large rotation in yaw,
- τ_4 : large translation on y-axis, large rotation in pitch,
- τ_5 : transformation (1), small roll rotation,
- τ_6 : transformation (2), small roll rotation.

We manually design the transformations, such that the main object or viewpoint of the scene is in full view at all times. To achieve this, for example when translating the camera upward, we apply a small rotation in pitch downward. This viewpoint requirement is assessed by manual inspection and takes a matter of seconds. By applying these transformations, we multiply the amount of test images in each scene sixfold as reported in Tbl. IV. Note that the transformations (1, 2), (3, 4) and (5, 6) increasingly deviate from the original camera path and should therefore produce more diverse image samples. We choose the following three image mutations by DeepXplore as our baseline, because from a practical point of view, they come closest to real-life failure modes in cameras:

- m_1 : changes in image brightness, e.g. caused by automated camera over-/underexposure,
- m_2 : applying one large patch of noisy pixels, e.g. caused by camera malfunction, transmittance failures or loose cables,
- m_3 : applying six small patches of black pixels, e.g. caused by dirt or stains on the camera lens.

a) Number of Inconsistencies: We report the number of inconsistencies per SUT in Fig. 10 and per scene in Fig. 11 according to our MT framework with three different threshold values for $\epsilon = [0.1, 0.2, 0.5]$. This means that we consider a deviation of a SUT metric by more than 10%, 20%, 50% an inconsistency in the behaviour of a SUT. The strictest test is $\epsilon = 0.1$ and should show the highest number of inconsistencies. Considering only NeRF-generated it can be said that transformations further away from the original path such as τ_4, τ_5, τ_6 show a higher number of inconsistencies per SUT for cosine similarity and IP spread. The biggest challenge for SUTs according to L2 norm seems to be the reality-to-

	Repeatability			IP Spread		
	PSNR	SSIM	LPIPS	PSNR	SSIM	LPIPS
SIFT	0.45 (1.71e-83)	0.57 (1.18e-144)	-0.52 (1.32e-114)	0.15 (4.21e-18)	0.22 (5.48e-37)	-0.18 (1.21e-25)
ORB	0.39 (1.37e-61)	0.56 (1.13e-135)	-0.47 (1.76e-89)	0.31 (1.01e-73)	0.30 (8.76e-70)	-0.38 (1.89e-112)
SuperPoint	0.38 (2.99e-59)	0.74 (2.66e-288)	-0.28 (6.20e-31)	0.12 (6.26e-13)	0.22 (2.94e-36)	-0.11 (1.11e-10)
UnSuperPoint	0.47 (8.34e-93)	0.70 (4.57e-244)	-0.44 (1.05e-77)	0.27 (2.50e-54)	0.20 (9.23e-32)	-0.30 (2.80e-71)
	Cosine Similarity			L2 Norm		
MobileNet	0.47 (4.14e-105)	0.46 (5.59e-104)	-0.39 (3.19e-69)	0.01 (4.49e-01)	0.02 (3.36e-01)	-0.01 (5.76e-01)
EfficientnetB0	0.27 (2.75e-34)	0.41 (3.96e-77)	-0.50 (5.99e-123)	0.01 (7.33e-01)	0.00 (9.24e-01)	-0.02 (3.06e-01)
Xception	0.31 (1.86e-45)	0.34 (5.50e-53)	-0.37 (4.79e-64)	0.00 (8.29e-01)	-0.01 (6.11e-01)	-0.01 (7.11e-01)
VGG16	0.52 (1.90e-136)	0.45 (8.61e-97)	-0.56 (1.10e-156)	-0.00 (8.12e-01)	-0.01 (6.50e-01)	-0.00 (8.63e-01)

TABLE III: Spearman Rank correlation coefficients and associated p-values (in brackets) between image quality metrics PSNR, SSIM, LPIPS and SUT metrics under the reality-to-NeRF domain shift in pose-equivalent images in S_{real} and S_{nerf} .

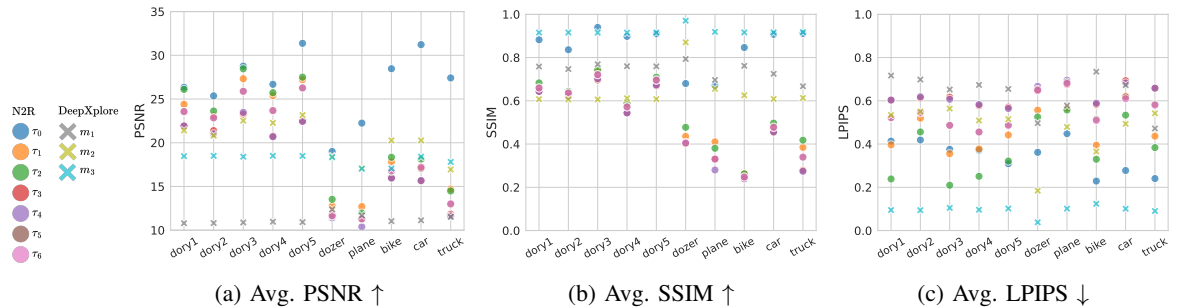


Fig. 8: Comparison of image metrics per scene under different pose transformations and mutations.



Fig. 9: Examples of inconsistent SUT behaviours: Image (a) transformed by τ_4 is classified as ImageNet1k class label “trash can” by MobileNet with 0.5285 confidence while having average image metric values (PSNR 15.77, SSIM 0.45, LPIPS 0.72). Image (b) transformed by τ_4 has a low repeatability score of 0.37 on SuperPoint. The low score is caused by a low agreement of points from the associated real image (green) compared to points found in this image (red). Image (b) has good metric values PSNR 35.12, SSIM 0.70, LPIPS 0.60.

NeRF shift in general. There is a difference in number of inconsistencies in DeepXplore mutations m_2, m_3 compared to m_1 . This is to be expected, since m_1 is a simple change in image brightness and should not challenge the SUT behaviour to a great extent. For L2 Norm, DeepXplore mutations m_2, m_3 quickly lose inconsistencies as the threshold ϵ increases. Generally, NeRF-images seem to target different aspects of SUT behaviours, that uncover a different range of inconsistencies than DeepXplore mutations. According to the IP spread metric, on average, IPDs seem more challenged by viewpoint changes of the NeRF-generated images than by mutated images.

b) Examples of Inconsistent Behaviour: See Fig. 9 for two examples of inconsistent SUT behaviour.

	dory1	dory2	dory3	dory4	dory5
#Test Images	1806	1980	2148	1818	2136
	plane	dozer	car	truck	bike
#Test Images	1902	2154	2286	2508	1818

TABLE IV: Number of NeRF-generated test images per scene.

C. RQ3: Efficiency

All NeRF trainings and image renderings are performed on two NVIDIA GPUs of type RTX 3090 Ti. Since the training and rendering times depend on the type of hardware available, we report carbon emissions to enable performance comparison. Once we have the fully trained models and rendered images of the scenes, the efficiency of executing N2R-Tester is predominantly determined by the efficiency of the SUTs, i.e. the time taken to process a test image, thus we consider it most appropriate to report the time taken for N2R-Tester to generate such test images.

a) NeRF Training Times \downarrow : See Tbl. I for a summary of the training times of 30k steps for each of the NeRF models.

b) NeRF Rendering Frames per Second (FPS) \uparrow : We report the average FPS for a trained NeRF model to render images at various image resolutions in Tbl. V. DeepXplore mutations can be artificially engineered with OpenCV at around 300 FPS. Compared to engineering a 3D environment in simulation, which requires hiring an experienced software engineer and many working hours, NeRF models still offer an effective shortcut to realistic 3D scene reconstruction.

c) Carbon Emissions \downarrow : An estimate of 300 hours of GPU time for NeRF training and 200 hours for image rendering were required on private infrastructure, having a carbon efficiency of 0.432 kgCO₂eq/kWh [38]. For our type of GPUs the total

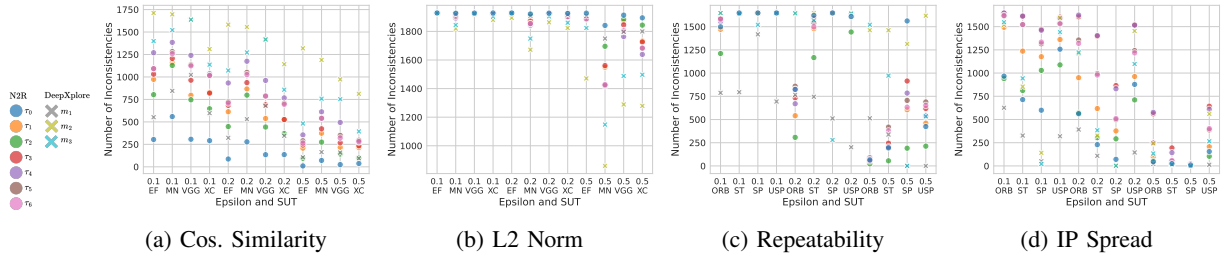


Fig. 10: Number of inconsistencies per metric per SUT under different pose transformations and mutations (EF=EfficientNet, MN=MobileNet, VGG=VGG16, XC=Xception, SP=SuperPoint, USP=UnSuperPoint).

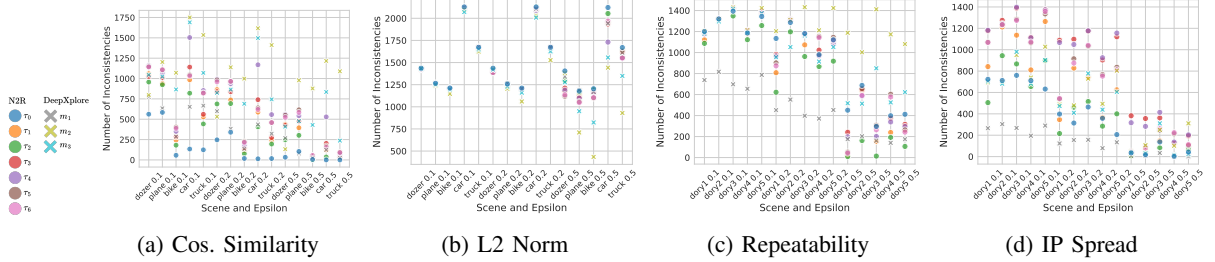


Fig. 11: Number of inconsistencies per metric per scene under different pose transformations and mutations.

Resolution	480 × 270	960 × 540	1920 × 1080
FPS	4.3	2.4	0.6

TABLE V: Rendering frame rates for a trained NeRF model at different image resolutions in frames per second (FPS) ↑.

emissions are estimated to be 75.6 kgCO₂eq by the Machine Learning Impact calculator, an equivalent of 305km driven by an average combustion-engine passenger car. Lower carbon emissions mean better performance. Notably, the vast majority of parameter fine-tuning was required for the underwater models. We suspect the challenge was aggravated by colmap’s difficulty to find coherent camera poses when faced with underwater images containing moving elements and backscattering light effects in the scenes. We consider it worth investigating if other NeRF architectures could mitigate these effects.

D. Threats to Validity and Limitations

a) Internal Validity: For AUV wall inspection, we configured the IPDs to produce hundred highest-confidence interest points (for performance reasons). IPDs can return more points, and it is possible that the behavior of an IPD on NeRF-generated and real images differs further on the omitted points. However, as the points are selected by confidence levels, the difference on the tail of the point distribution should be of decreasing importance.

b) External Validity: The test results with NeRF-generated data for IPDs and classifiers do not necessarily transfer to other scenes, other IPDs, other classification domains, and other classification models. This is an inherent problem with machine language models. So far the only way to increase confidence of transferability is to accumulate experience with more domains, more models, and more vision components. In our experiments, we have used two vastly different visual tasks (classification and interest-point detection) and used data sets from different domains and different locations. We have



Fig. 12: Examples of NeRF artifacts (enlarged, best seen on screen). Top left: a real image of a reflective surface. Top right: an imprecise rendering in `car` of the same view as top left. Bottom left: An example of an under-defined pixel patch in `bike`. Bottom right: An example of a ghost wall in `dory1`.

used both DNN-based and non-DNN-based IPDs, and large and small classifier models, to increase generalisability.

c) Limitations: With a trained NeRF model we can only produce test images of one specific instance of a scene or object. Generally, DNNs are trained to classify a wide range of visually distinct instances of the same class. Still, NeRF models can serve as a valuable test image generation technique in scenarios where a particular subset of classes is of interest, for example in the case of transfer learning.

Similarly to any DNN, the output quality during inference relies heavily on the relevant samples received during training. For NeRFs, the visual fidelity in the generated images depends on the number of ray samples in proximity. Consequently, the images of the original camera poses (\mathbf{x}, \mathbf{d}) of the real images in the scene $i_{\text{real}} \in \mathcal{S}$ are most likely to be most accurately represented in the NeRF model. Conversely, the further we deviate from these poses, the likelihood of rendering under-defined pixels increases.

VII. RELATED WORK

a) Metamorphic testing for vision components: Since DNNs are efficient in processing image data, there is a trend to replace traditional vision-based navigational algorithms by end-to-end trained neural networks. It is thus crucial to consider the challenges associated with testing neural networks in general. Methods such as DeepXplore [6] and DeepTest [7] attempt to uncover erroneous behaviour of neural networks by synthesising inputs based on maximising neuron coverage. However, while doing this, they do not respect the geometric properties of the scene, so the generated sequences of images do not guarantee spatio-temporal consistency. DeepRoad is a MT framework producing test images with different weather effects via domain adaptation with GANs [12]. The images are transformed on a per-frame basis, so DeepRoad is limited to test of aspects such as steering angle accuracy. It does not offer geometric consistency for a stream of frames, hence it is unsuitable for testing vSLAM components such as IPDs processing consecutive frames. MT has been applied to evaluate aerial drone control policies in simulation [39]. Here, the SUT is the drone controller and test inputs are various states of the simulated environment in combination with a mission, e.g. ‘take-off’ or ‘fly-to-location’ This line of work was extended to develop MRs for testing obstacle-avoidance algorithms for single and multiple agents in simulation [40]. Our work addresses testing image processing algorithms with images such as test inputs, hence posing as a distinct approach to applying metamorphic testing in the robotics domain. To the best of our knowledge, we are the first to investigate how NeRFs can be applied in test image generation.

b) NeRFs for localisation, navigation and scene representation: The potential applications of NeRFs in the robotics domain are still largely unexplored [41]. NeRFs can improve vision-based trajectory planners and collision avoidance for aerial drones [42]. NeRF2Real fuses a NeRF with a physics simulator to achieve fast renderings of a scene as well as modeling of dynamic objects, the robot body, interactions, and collisions [43]. SPARTN is a data augmentation technique for an eye-in-hand robotic arm that feeds NeRF-generated visual samples of grasping behaviours into a robotic imitation learning pipeline [44]. Notably, SPARTN and NeRF2Real conduct evaluations on physical robots and hence directly tackle the “simulation-to-reality” gap. While these works enhance robotics functionality, we focus on automating meaningful test data generation for systematic vision task testing in robotics. Several works address the degradation of NeRFs visual clarity due to inaccurate or inaccessible camera poses during training. Bundle-Adjusting Neural Radiance Fields [45] optimize jointly for camera poses and visual input, therefore alleviating the dependence on the accuracy of Structure-from-Motion tools, and enabling reconstruction from imperfect or even unknown camera poses [17]. Renderable Neural Radiance Maps enhance NeRFs’ ability to map visual input into latent spaces, providing additional 3D scene information for improved localization [46]. Loc-NeRF combines Monte-Carlo localisation with a pre-trained NeRF for fast localisation without depending on a

perfect initial pose estimate [47]. These methods improve visual pose estimation and navigation through scenes, distinct from independently building realistic test mechanisms to uncover faulty behaviours of navigation components, as presented in this paper. NeRF-SLAM uses the output of dense monocular SLAM, i.e. depth maps and camera poses with the associated uncertainties for NeRF training [48]. NeRF-SLAM addresses neither testing nor improve SLAM with NeRFs, as the name may suggest. It aims to produce renderings with high photometric and geometric accuracy. SeaThru-NeRFs improve generated images by differentiating back-scatter effects from large unbounded underwater scenes [49]. In this work, we used small and bounded underwater scenes where these advantages did not offer significant visual improvements. Beyond-NeRF Underwater targets colour correction of images captured by a bottom-facing AUV camera [50]. These typically feature an artificial light source causing a high concentration of unexposed pixels, which makes them unsuitable in our context. Finally, we were unable to find and access source code for WaterNeRF [51] and WaterHE-NeRF [52].

VIII. CONCLUSION

N2R-Tester is a metamorphic testing and test data synthesis method for perception components of autonomous vehicles. Like other metamorphic methods, it does not use domain-specific or project-specific rules to specify tests. N2R-Tester offers a plethora of advantages over other image generation techniques for navigation applications. First, it grants precise control over image transformations, as opposed to models such as GANs. Self-contained image rotations are fundamentally not possible using real images alone, without loss of information; as soon as we rotate an image for example in OpenCV, we lose pixels in the image corners and need to zoom in, extrapolate, or inpaint to get a coherent image. Second, unlike other computer graphics methods, such as textured meshes combined with sophisticated rendering engines, it does not require explicit 3D models of the scene. A NeRF model is a continuous function approximation capable of implicitly representing complex scenes with arbitrary shapes, appearances and textures, which offers great flexibility over traditional techniques. Third, it does not require human annotation. A NeRF model learns to represent a 3D scene solely based on real 2D image inputs. Fourth, N2R-Tester does not directly rely on image fidelity metrics such as PSNR, SSIM, and LPIPS for assessing image realness on a per-sample basis, rather they act as more global indicators of satisfactory NeRF in-training-evaluation. N2R-Tester can be potentially extended to test stereo-vision, as it can render two offset camera views. NeRFs inherently model depth in the α -channel of the output layer and could therefore also be used to test depth perception. Finally, NeRFs could be replaced by newer 3D reconstruction models such as Gaussian Splatting [53].

Acknowledgments: This project has received funding from the European Union’s Horizon 2020 research and innovation programme under the Marie Skłodowska-Curie grant agreement No 956200. Fragments of Fig. 2 are generated with DALL-E by Open AI.

REFERENCES

- [1] L. Carroll, *Alice's Adventures in Wonderland.*, 1865.
- [2] S. Arnold and L. Medagoda, "Robust model-aided inertial localization for autonomous underwater vehicles," in *2018 IEEE international conference on robotics and automation (ICRA)*. IEEE, 2018, pp. 4889–4896.
- [3] B. Mildenhall, P. P. Srinivasan, M. Tancik, J. T. Barron, R. Ramamoorthi, and R. Ng, "Nerf: Representing scenes as neural radiance fields for view synthesis," *Communications of the ACM*, vol. 65, no. 1, pp. 99–106, 2021.
- [4] O. Álvarez-Tuñón, H. Kanner, L. R. Marnet, H. X. Pham, J. le Fevre Sejersen, Y. Brodskiy, and E. Kayacan, "MIMIR-UW: A multipurpose synthetic dataset for underwater navigation and inspection," in *IROS*, 2023, pp. 6141–6148. [Online]. Available: <https://doi.org/10.1109/IROS55552.2023.10341436>
- [5] I. J. Goodfellow, J. Shlens, and C. Szegedy, "Explaining and harnessing adversarial examples," *arXiv preprint arXiv:1412.6572*, 2014.
- [6] K. Pei, Y. Cao, J. Yang, and S. Jana, "Deepxplore: Automated whitebox testing of deep learning systems," in *Proceedings of the 26th Symposium on Operating Systems Principles*. ACM, 2017, pp. 1–18.
- [7] Y. Tian, K. Pei, S. Jana, and B. Ray, "Deeptest: Automated testing of deep-neural-network-driven autonomous cars," in *Proceedings of the 40th international conference on software engineering*, 2018, pp. 303–314.
- [8] X. Xie, L. Ma, F. Juefei-Xu, H. Chen, M. Xue, B. Li, Y. Liu, J. Zhao, J. Yin, and S. See, "Deephunter: Hunting deep neural network defects via coverage-guided fuzzing," *arXiv preprint arXiv:1809.01266*, 2018.
- [9] T. Woodlief, S. Elbaum, and K. Sullivan, "Semantic image fuzzing of AI perception systems," pp. 1958–1969, 2022.
- [10] T. Zohdinasab, V. Riccio, A. Gambi, and P. Tonella, "Deephyperion: exploring the feature space of deep learning-based systems through illumination search," in *Proceedings of the 30th ACM SIGSOFT International Symposium on Software Testing and Analysis*, 2021, pp. 79–90.
- [11] T. Zohdinasab, V. Riccio, and P. Tonella, "Deepatash: Focused test generation for deep learning systems," in *ISSTA '23*, 2023, pp. 954–966.
- [12] M. Zhang, Y. Zhang, L. Zhang, C. Liu, and S. Khurshid, "Deeproad: Gan-based metamorphic testing and input validation framework for autonomous driving systems," pp. 132–142, 2018.
- [13] S. Dola, M. B. Dwyer, and M. L. Soffa, "Distribution-aware testing of neural networks using generative models," in *2021 IEEE/ACM 43rd International Conference on Software Engineering (ICSE)*. IEEE, 2021, pp. 226–237.
- [14] Z. Wang and A. C. Bovik, "Mean squared error: Love it or leave it? a new look at signal fidelity measures," *IEEE signal processing magazine*, vol. 26, no. 1, pp. 98–117, 2009.
- [15] R. Zhang, P. Isola, A. A. Efros, E. Shechtman, and O. Wang, "The unreasonable effectiveness of deep features as a perceptual metric," in *Proceedings of the IEEE conference on computer vision and pattern recognition*, 2018, pp. 586–595.
- [16] T. Y. Chen, F.-C. Kuo, H. Liu, P.-L. Poon, D. Towey, T. Tse, and Z. Q. Zhou, "Metamorphic testing: A review of challenges and opportunities," *ACM Computing Surveys (CSUR)*, vol. 51, no. 1, pp. 1–27, 2018.
- [17] J. L. Schonberger and J.-M. Frahm, "Structure-from-motion revisited," pp. 4104–4113, 2016.
- [18] M. Tancik, E. Weber, E. Ng, R. Li, B. Yi, T. Wang, A. Kristoffersen, J. Austin, K. Salahi, A. Ahuja *et al.*, "Nerfstudio: A modular framework for neural radiance field development," pp. 1–12, 2023.
- [19] D. DeTone, T. Malisiewicz, and A. Rabinovich, "Superpoint: Self-supervised interest point detection and description," pp. 224–236, 2018.
- [20] P. H. Christiansen, M. F. Kragh, Y. Brodskiy, and H. Karstoft, "Unsuperpoint: End-to-end unsupervised interest point detector and descriptor," 2019.
- [21] D. G. Lowe, "Distinctive image features from scale-invariant keypoints," *International journal of computer vision*, vol. 60, pp. 91–110, 2004.
- [22] E. Rublee, V. Rabaud, K. Konolige, and G. Bradski, "Orb: An efficient alternative to sift or surf," *Ieee*, pp. 2564–2571, 2011.
- [23] G. Bradski, "The opencv library," *Dr. Dobbs's Journal: Software Tools for the Professional Programmer*, vol. 25, no. 11, pp. 120–123, 2000.
- [24] Magic Leap, Inc., "Superpoint pretrained network," <https://github.com/magicleap/SuperPointPretrainedNetwork>, 2023, accessed: 2023-03-14.
- [25] A. G. Howard, M. Zhu, B. Chen, D. Kalenichenko, W. Wang, T. Weyand, M. Andreetto, and H. Adam, "Mobilenets: Efficient convolutional neural networks for mobile vision applications," *arXiv preprint arXiv:1704.04861*, 2017.
- [26] M. Tan and Q. Le, "Efficientnet: Rethinking model scaling for convolutional neural networks," in *International conference on machine learning*. PMLR, 2019, pp. 6105–6114.
- [27] F. Chollet, "Xception: Deep learning with depthwise separable convolutions," in *Proceedings of the IEEE conference on computer vision and pattern recognition*, 2017, pp. 1251–1258.
- [28] K. Simonyan and A. Zisserman, "Very deep convolutional networks for large-scale image recognition," *arXiv preprint arXiv:1409.1556*, 2014.
- [29] F. Chollet *et al.*, "Keras," <https://keras.io>, 2015.
- [30] J. Deng, W. Dong, R. Socher, L.-J. Li, K. Li, and L. Fei-Fei, "Imagenet: A large-scale hierarchical image database," in *2009 IEEE conference on computer vision and pattern recognition*. Ieee, 2009, pp. 248–255.
- [31] F. Chollet *et al.*, "Keras application details," <https://keras.io/api/applications/>, 2015, accessed: 1.April 2024.
- [32] C. Schmid, R. Mohr, and C. Bauckhage, "Evaluation of interest point detectors," *International Journal of computer vision*, vol. 37, no. 2, pp. 151–172, 2000.
- [33] O. Bailo, F. Rameau, K. Joo, J. Park, O. Bogdan, and I. S. Kweon, "Efficient adaptive non-maximal suppression algorithms for homogeneous spatial keypoint distribution," *Pattern Recognition Letters*, vol. 106, pp. 53–60, 2018.
- [34] Z. Yang, J. Shi, M. H. Asyofi, and D. Lo, "Revisiting neuron coverage metrics and quality of deep neural networks," in *2022 IEEE International Conference on Software Analysis, Evolution and Reengineering (SANER)*. IEEE, 2022, pp. 408–419.
- [35] F. Warburg, E. Weber, M. Tancik, A. Holynski, and A. Kanazawa, "Nerfbusters: Removing ghostly artifacts from casually captured nerfs," in *Proceedings of the IEEE/CVF International Conference on Computer Vision*, 2023, pp. 18 120–18 130.
- [36] H. Xu, T. Alldieck, and C. Sminchisescu, "H-nerf: Neural radiance fields for rendering and temporal reconstruction of humans in motion," *Advances in Neural Information Processing Systems*, vol. 34, pp. 14 955–14 966, 2021.
- [37] S. Fridovich-Keil, G. Meanti, F. R. Warburg, B. Recht, and A. Kanazawa, "K-planes: Explicit radiance fields in space, time, and appearance," pp. 12 479–12 488, 2023.
- [38] A. Lacoste, A. Luccioni, V. Schmidt, and T. Dandres, "Quantifying the carbon emissions of machine learning," *arXiv preprint arXiv:1910.09700*, 2019.
- [39] M. Lindvall, A. Porter, G. Magnusson, and C. Schulze, "Metamorphic model-based testing of autonomous systems," in *2017 IEEE/ACM 2nd International Workshop on Metamorphic Testing (MET)*, IEEE. IEEE, 2017, pp. 35–41.
- [40] J. G. Adigun, L. Eisele, and M. Felderer, "Metamorphic testing in autonomous system simulations," *IEEE*, pp. 330–337, 2022.
- [41] E. Šlapak, E. Pardo, M. Dopiriak, T. Maksymyuk, and J. Gazda, "Neural radiance fields in the industrial and robotics domain: applications, research opportunities and use cases," 2023.
- [42] M. Adamkiewicz, T. Chen, A. Caccavale, R. Gardner, P. Culbertson, J. Bohg, and M. Schwager, "Vision-only robot navigation in a neural radiance world," *IEEE Robotics and Automation Letters*, vol. 7, no. 2, pp. 4606–4613, 2022.
- [43] A. Byravan, J. Humplik, L. Hasenclever, A. Brussee, F. Nori, T. Haarnoja, B. Moran, S. Bohez, F. Sadeghi, B. Vujatovic *et al.*, "Nerf2real: Sim2real transfer of vision-guided bipedal motion skills using neural radiance fields," in *2023 IEEE International Conference on Robotics and Automation (ICRA)*. IEEE, 2023, pp. 9362–9369.
- [44] A. Zhou, M. J. Kim, L. Wang, P. Florence, and C. Finn, "Nerf in the palm of your hand: Corrective augmentation for robotics via novel-view synthesis," in *Proceedings of the IEEE/CVF Conference on Computer Vision and Pattern Recognition*. IEEE, 2023, pp. 17 907–17 917.
- [45] C.-H. Lin, W.-C. Ma, A. Torralba, and S. Lucey, "Barf: Bundle-adjusting neural radiance fields," in *Proceedings of the IEEE/CVF International Conference on Computer Vision*, 2021, pp. 5741–5751.
- [46] O. Kwon, J. Park, and S. Oh, "Renderable neural radiance map for visual navigation," in *Proceedings of the IEEE/CVF Conference on Computer Vision and Pattern Recognition*, 2023, pp. 9099–9108.
- [47] D. Maggio, M. Abate, J. Shi, C. Mario, and L. Carloni, "Loc-nerf: Monte carlo localization using neural radiance fields," in *2023 IEEE International Conference on Robotics and Automation (ICRA)*. IEEE, 2023, pp. 4018–4025.
- [48] A. Rosinol, J. J. Leonard, and L. Carloni, "Nerf-slam: Real-time dense monocular slam with neural radiance fields," in *2023 IEEE/RSJ*

International Conference on Intelligent Robots and Systems (IROS).
IEEE, 2023, pp. 3437–3444.

- [49] D. Levy, A. Peleg, N. Pearl, D. Rosenbaum, D. Akkaynak, S. Korman, and T. Treibitz, “Seathru-nerf: Neural radiance fields in scattering media,” pp. 56–65, 2023.
- [50] T. Zhang and M. Johnson-Roberson, “Beyond nerf underwater: Learning neural reflectance fields for true color correction of marine imagery,” *IEEE Robotics and Automation Letters*, 2023.
- [51] A. V. Sethuraman, M. S. Ramanagopal, and K. A. Skinner, “Waternerf: Neural radiance fields for underwater scenes,” in *OCEANS 2023-MTS/IEEE US Gulf Coast*. IEEE, 2023, pp. 1–7.
- [52] J. Zhou, T. Liang, Z. He, D. Zhang, W. Zhang, X. Fu, and C. Li, “Waterhe-nerf: Water-ray tracing neural radiance fields for underwater scene reconstruction,” *arXiv preprint arXiv:2312.06946*, 2023.
- [53] B. Kerbl, G. Kopanas, T. Leimkühler, and G. Drettakis, “3d gaussian splatting for real-time radiance field rendering,” *ACM Transactions on Graphics (ToG)*, vol. 42, no. 4, pp. 1–14, 2023.